J. Fluid Mech. (2006), *vol.* 557, *pp.* 337–346. © 2006 Cambridge University Press
doi:10.1017/S0022112006000218 Printed in the United Kingdom

The motion of a rough particle in a Stokes flow adjacent to a boundary

By L. YANG[1]†, J. R. T. SEDDON[1], T. MULLIN[1], C. DEL PINO[1]‡ AND J. ASHMORE[2]¶

[1]Manchester Centre for Nonlinear Dynamics, University of Manchester, Oxford Road, Manchester M13 9PL, UK
[2]Department of Applied Mathematics and Theoretical Physics, University of Cambridge, Wilberforce Road, Cambridge CB3 0WA, UK

(Received 3 October 2005 and in revised form 29 March 2006)

Results are presented of experimental investigations into the motion of a heavy sphere in a rotating cylinder which is completely filled with highly viscous fluid. For a given cylinder rotation rate, the sphere adopts a fixed position and rotates adjacent to the cylinder wall. For the case of a smooth sphere the motion is consistent with that predicted by a Stokes flow model. Artificially roughened spheres exhibit particle–boundary contact caused by impacts of surface asperities with the boundary for low cylinder surface speeds. For higher cylinder surface speeds the behaviour of the roughened spheres crosses smoothly from the particle–boundary contact regime to motion with hydrodynamically lubricated flow.

1. Introduction

The motion of a sphere in a Stokes flow near to a boundary is of fundamental importance since it arises in many industrial problems, such as bearings, cleaning processes, colloidal suspensions, fluidization and filtration (Dowson & Taylor 1979; Segre, Herbolzheimer & Chaikin 1997). The simplest experimental system that can be used to realize this kind of flow is that of a sphere immersed in a viscous fluid moving down an inclined plane (Smart, Beimfohr & Leighton 1993; Galvin, Zhao & Davis 2001; Prokunin 2004). This apparently simple configuration has been used to develop models for the motion of both smooth and rough spheres.

Goldman, Cox & Brenner (1967) modelled the translational and rotational motion of a perfectly smooth sphere near to a vertical smooth boundary by considering torque and force balances tangential to the boundary. However, owing to the reversibility of the Stokes equations and the local symmetry of the flow geometry, this model predicts no net hydrodynamical force normal to the boundary. A perfectly smooth sphere will asymptotically approach the wall if the boundary is inclined at an angle less than 90° to the horizontal. The resolution of this problem for the case of a heavy sphere was provided by Ashmore, del Pino & Mullin (2005) who showed that cavitation in the lubrication layer breaks the symmetry of the flow so that the flow exerts a normal force on the sphere, which can balance the normal component of the sphere's weight.

† Present address: Huazhong University of Science and Technology, Wuhan, 430074, Hubei, China.
‡ Present address: ETSII, Universidad de Malaga, Spain.
¶ Present address: TIAX LLC, 15 Acorn Park, Cambridge, MA 02140, USA.

Hence, a cavity exists in the lubricating layer between the sphere and the moving boundary, and details such as the size and position of the bubble have been verified experimentally.

Now that the motion of a smooth heavy sphere near to a boundary in a Stokes flow is understood, one question to ask concerns the role of surface roughness. It is well known (see e.g. Acheson 1990) that there is a mathematical singularity when the distance between a sphere and boundary asymptotically approaches zero, i.e. when the lubricating layer depth tends to zero. Hence, a perfect sphere moving towards a smooth wall can theoretically never make contact. Similarly, a perfect sphere touching a smooth wall can never break contact. However, experimental data confirm that particle–boundary contact can be made and broken and this is believed to arise from the presence of surface roughness. Smart *et al.* (1993) provide a model to describe such effects on spheres moving near to a boundary in a Stokes flow. In the model the motion is considered to comprise tangential motion arising from slip between the sphere and plane, normal motion of a part of the sphere surface relative to the plane arising from rotation of the sphere, and pressure-driven channel flow in the lubrication layer between the sphere and plane. Smart *et al.* (1993) use a classical mechanics approach to model the roughness effects by introducing a frictional force into the theory of Goldman *et al.* (1967). This opposes the translational motion of the sphere where a coefficient of friction is assumed to exist between the sphere and boundary. The precise value of the coefficient of friction is obtained by fitting with experimental data. Galvin *et al.* (2001) develop this model and use it to describe the motion of a rough sphere in a Stokes flow close to a smooth boundary. Specifically, they include two distinctive roughness levels on the sphere.

The present study is an investigation into the effects of roughness levels on a heavy sphere moving near to a boundary in a Stokes flow, where the measure of roughness ϵ is defined as the ratio of the maximum peak–valley depth of the rough asperities to the sphere diameter. The system consists of a horizontal rotating cylinder filled with very viscous fluid. A roughened steel sphere was placed within the fluid and found to rotate at a fixed point adjacent to the upward moving wall in the lower quadrant of the cylinder for a set rotation rate. When the cylinder was made to rotate faster the sphere moved up the wall to new fixed points until it reached 90°, where upon it fell from the wall and oscillatory motion set in. This in turn could lead to periodic particle–particle interactions when two spheres were present and spatio-temporal chaos with three spheres, all of which are described in detail in Mullin *et al.* (2005).

We will concern ourselves with fixed-point behaviour where the sphere sits in the lower quadrant of the cylinder. This is analogous to a sphere rolling down an inclined plane: where the plane can lie at an angle between 0 and 90°, the tangent to the sphere at the point of nearest approach to the cylinder wall can also lie between 0 and 90°. Differences between these two systems are discussed in more detail in § 3. Our experimental observations show that particle–boundary contact is possible for roughened spheres at small angles, but their motion can be described by the hydrodynamic model of Ashmore *et al.* (2005) over a wide range of angles up the cylinder wall. Moreover, there is a smooth crossover between the particle–boundary contact and the hydrodynamic regimes.

2. Hydrodynamic model for smooth spheres adjacent to an inclined plane

It is useful to review the hydrodynamic model for a smooth sphere adjacent to an inclined plane in a Stokes flow, of Ashmore *et al.* (2005). A smooth sphere of radius

a and density ρ_s rotates at a rate ω in a semi-infinite fluid bath close to a boundary. The fluid has viscosity μ and density ρ_f and the boundary is inclined at angle θ, moving at velocity U. The sphere sits adjacent to the boundary, separated by a thin lubrication layer of thickness h_0, and its motion can be found from the lubrication approximation of the Stokes equations. The key idea is that the pressure distribution in the lubricating layer in the expansion region of the flow drops below the negative vapour pressure of the fluid. A vapour cavity is formed and the pressure distribution is truncated at the vapour pressure. The symmetry of the problem is then broken and a net normal force exists thereby preventing sphere/boundary contact.

We choose a polar coordinate system (r, ϕ) with origin at the point of closest approach between the sphere and boundary and with the angle ϕ equal to zero in the opposite direction to boundary motion. The deviation from atmospheric pressure in the lubricating layer is $p(r, \phi)$, the difference between atmospheric pressure and vapour pressure is p_b, and the density difference is $\Delta\rho = \rho_s - \rho_f$. Variables are non-dimensionalized as follows:

$$\left.\begin{aligned} \mathscr{U} &= \frac{\mu U}{\Delta\rho g a^2}, \qquad \Omega = \frac{\omega a}{U}, \qquad \mathscr{H}_0 = \frac{h_0}{a}, \\ \mathscr{P}_b &= \frac{p_b}{\Delta\rho g a}, \qquad \mathscr{P} = \frac{p}{\Delta\rho g a}, \qquad R = \frac{r}{(2h_0 a)^{1/2}}. \end{aligned}\right\} \tag{2.1}$$

Ashmore *et al.* (2005) argue that the tangential force and torque balances on the sphere will not be greatly affected by the presence of the vapour bubble so that the asymptotic solutions of Goldman *et al.* (1967) should still be valid:

$$\frac{16\pi}{5}\left(1 - \frac{\Omega}{4}\right)\mathscr{U}\ln\left(\frac{1}{\mathscr{H}_0}\right) + 6\pi(0.9588 + 0.2526\Omega)\mathscr{U} = \frac{4\pi}{3}\sin\theta, \tag{2.2}$$

$$\frac{1}{10}(1 - 4\Omega)\ln\left(\frac{1}{\mathscr{H}_0}\right) - 0.1895 - 0.3817\Omega = 0. \tag{2.3}$$

The force balance normal to the plane is

$$F_N = 2\mathscr{H}_0\int_0^{2\pi}\int_0^{\sqrt{1/2\mathscr{H}_0}} P\,R\,\mathrm{d}R\,\mathrm{d}\phi = \frac{4\pi}{3}\cos\theta \tag{2.4}$$

where F_N has been non-dimensionalized by $\Delta\rho g a^3$. The pressure distribution in the gap is given by the lubrication pressure P_{lub}, truncated at the vapour pressure: $P(R, \phi) = \max\{P_{lub}(R, \phi), -\mathscr{P}_b\}$, where

$$P_{lub}(R, \phi) = \frac{6\sqrt{2}(1 + \Omega)\mathscr{U}}{5\mathscr{H}_0^{3/2}}\frac{R}{(1 + R^2)^2}\cos\phi. \tag{2.5}$$

The equations of motion can be solved using a Newton–Rhapson scheme to find $\mathscr{U}$, Ω and $\mathscr{H}_0$, as well as an estimate for the vapour bubble size, for a given value of the vapour pressure $\mathscr{P}_b$.

3. Experimental setup

The experiments were carried out using a glass cylinder of length 195 mm and inner radius 60.00 ± 0.02 mm, which was precision bored to a surface roughness of $20 \pm 4 \times 10^{-6}$ defined as the ratio of maximum peak–valley depth to cylinder diameter and measured using a surface roughness comparator. A schematic diagram of the

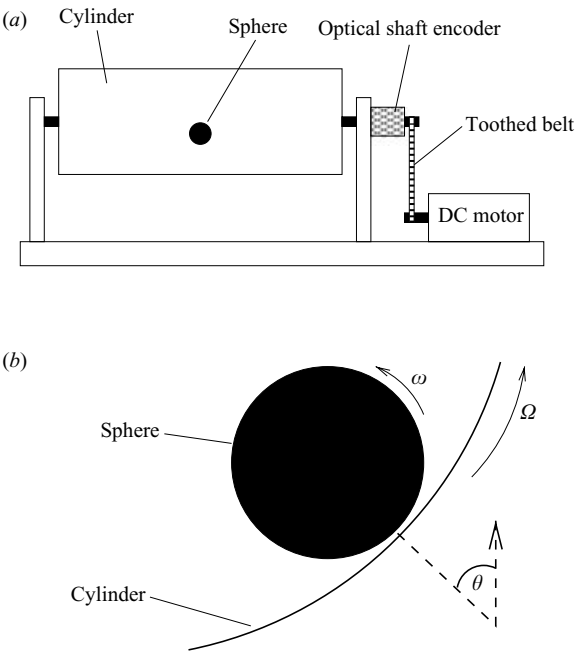

FIGURE 1. Overview of the experimental apparatus. (*a*) Front view showing the sphere inside the cylinder. (*b*) Sphere rotating close to the cylinder wall in the fixed-point regime.

apparatus is given in figure 1(*a*). The end caps of the cylinder contained centred ball races which were used to mount the cylinder horizontally and this was checked with a precision level. The cylinder was rotated at constant angular velocity using a DC feedback controlled motor connected via a gear box and toothed-belt drive. Its rotational frequency was monitored using an optical shaft encoder and was found to be constant to within ± 0.001 Hz. Sphere rotation rates were estimated using a stopwatch to measure the passage time of lightly applied pen marks on the sphere to pass a known position averaged over 50 orbits.

The two fluids used in this study were silicone oil and glycerine, held at a constant temperature to an accuracy of $\pm 0.1\,^{\circ}$C. The kinematic viscosities were found by interpolating viscosity–temperature calibration charts provided by the fluid manufacturers and the values used in the experiments described here were 813 and 1192 $\mathrm{mm^2\,s^{-1}}$ for glycerine (corresponding to temperatures of 23.6 and 19.5 °C respectively) and 1089 $\mathrm{mm^2\,s^{-1}}$ for silicone oil (only one temperature was used for silicone oil, 21.7 °C). Prokunin (2004) showed that air dissolved in the system can form a bubble in the lubrication layer between the sphere and boundary. Degassing the fluids before carrying out the experiments reduced any dissolved air that may have otherwise interfered with the sphere motion. The effects caused by gassy fluids will be discussed in § 4.

The steel spheres used in the experiments had densities of $7800 \pm 5\,\mathrm{kg\,m^{-3}}$ and diameters of 6.0, 15.8 and 25.0 mm. Tolerances on the diameter of the spheres were 2.5 μm and the inherent roughness of the smooth spheres was $\epsilon = 5.0 \pm 0.2 \times 10^{-6}$. In addition to these, a 15.8 mm sphere and three 25 mm spheres were artificially roughened. This was done by uniformly grinding the spheres in a rotating drum with grits of well-defined sizes over a period of 3 days. The 25 mm artificially roughened

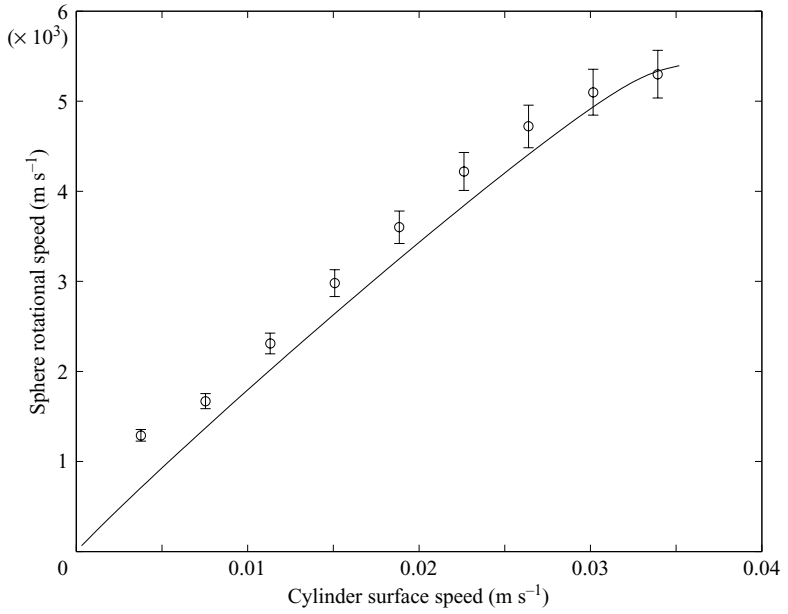

FIGURE 2. Relationship between the cylinder surface speed and sphere rotational speed for the 6 mm sphere. The solid curve represents the theoretical predictions of Ashmore *et al.* (2005). Discrepancies between the experimental data and theoretical predictions are of order the size of the experimental uncertainty when this small sphere is used, suggesting that curvature effects or the outer flow field are the cause of the discrepancy between prediction and experiment in figure 3.

spheres had measured roughnesses of $\epsilon = 84 \pm 4 \times 10^{-6}$, $164 \pm 4 \times 10^{-6}$ and $440 \pm 20 \times 10^{-6}$ and the 15.8 mm sphere was roughened to $\epsilon = 481 \pm 19 \times 10^{-6}$. Surface roughness was measured using an optical interferometric profilometry device where a light beam was reflected off the sphere and its surface topography was recorded by measuring the scattered light.

For slow cylinder rotation rates the spheres rotated at fixed points up the cylinder wall, separated from the boundary by a thin lubrication layer as shown schematically in figure 1(*b*) and described in detail by Mullin *et al.* (2005). All experiments were carried out in the single-sphere fixed-point regime. Increasing the cylinder surface speed increased the angle up the wall at which the sphere was stationary until, at 90°, the motion of the sphere became unstable and it began to oscillate.

The model of Ashmore *et al.* (2005) describes the translation and rotation of a sphere down an inclined plane, with boundary conditions that all motion tends to zero in the outer flow field. In our experiments the inclined plane is replaced with a cylinder of finite curvature so the outer flow field is limited by the cylinder diameter and effects due to curvature can exist. Moreover, after one complete rotation of the cylinder the sphere travels in the wake created from its previous passing of that point on the cylinder wall. We found quite a large discrepancy between theoretical prediction and experimental measurement for the 25 mm diameter spheres but also found that this discrepancy reduced with reducing sphere size. A graph of sphere rotational speed as a function of cylinder surface speed for the 6 mm sphere in silicone oil is plotted in figure 2, with excellent agreement between theoretical predictions and experimental measurement. Hence, this suggests that a sizeable amount of the discrepancy is due to either the finite curvature of the drum or the outer flow field.

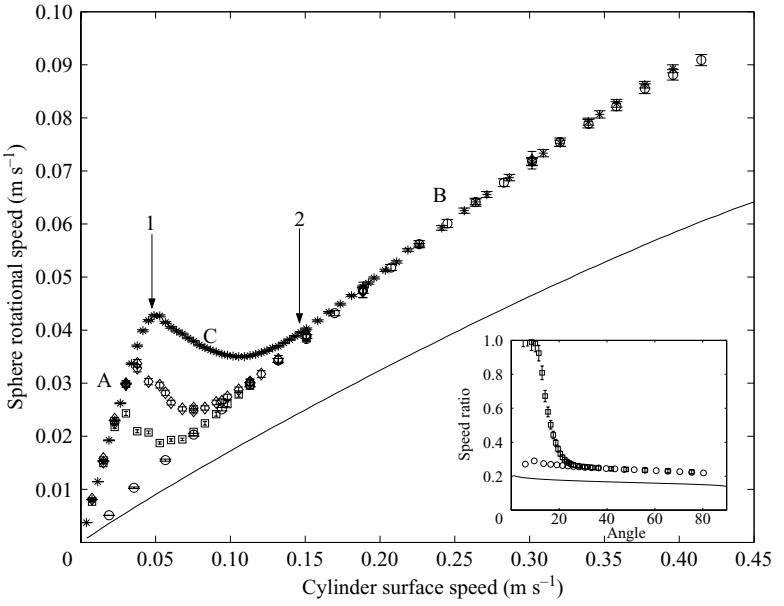

FIGURE 3. Relationship between the cylinder surface speed and sphere rotational speeds for the 25 mm spheres with roughnesses of $\epsilon = 5 \times 10^{-6}$ (circles), 84×10^{-6} (squares), 164×10^{-6} (diamonds) and 440×10^{-6} (stars). The motion can be described in terms of a particle–boundary contact regime (A) and a hydrodynamic regime (B) with a smooth crossover (C) between the two. The transition between region A and C is labelled 1 and that between B and C is labelled 2 for the $\epsilon = 440 \times 10^{-6}$ sphere. The solid curve represents the theoretical predictions of Ashmore *et al.* (2005). The cylinder was completely filled with glycerine and held at a constant temperature of $23.6 \pm 0.1\,^{\circ}$C, corresponding to a viscosity of $813 \pm 7\,\mathrm{mm^2\,s^{-1}}$. Inset is the ratio of sphere rotational speed to cylinder surface speed as a function of position angle for the $\epsilon = 5 \times 10^{-6}$ (circles) and $\epsilon = 440 \times 10^{-6}$ (squares) spheres.

4. Results and discussion

Plots of the rotational speed of the 25 mm diameter spheres versus that of the cylinder are shown in figure 3 where each data point was recorded at a fixed point of the sphere. The three roughened spheres possessed quite different behaviour from the smooth sphere at low cylinder rotation rates. Rough spheres rotated at the same speed as the boundary, as may be seen in region A of figure 3 where the gradient of the slope is equal to 1, plotted as an inset to figure 3, indicating sphere–wall contact. This suggests that continual impacts occurred between rough asperities on the sphere and cylinder wall and the sphere was driven by frictional contact with the boundary. However, a vapour cavity was observed over the entire rotational speed range, i.e. even in the sphere–boundary contact regime.

At faster cylinder rotation rates the roughened spheres began to slip with respect to the cylinder wall and departed from the sphere–boundary contact regime. A smooth transition (region C) was found between the contact and the hydrodynamic regimes where the latter is in accord with previous results for smooth spheres (region B). Slippage between the rough spheres and boundary first occurred at angles of 11°, 13° and $15 \pm 2\,^{\circ}$ for the $\epsilon = 84 \times 10^{-6}$, 164×10^{-6} and 440×10^{-6} spheres respectively and departure from the contact regime appeared sharp. The motion of the spheres crossed over to the hydrodynamic limit gradually and joined it at angles of 18°, 22° and $26 \pm 2\,^{\circ}$ for the three increasing roughnesses. The corresponding angles at

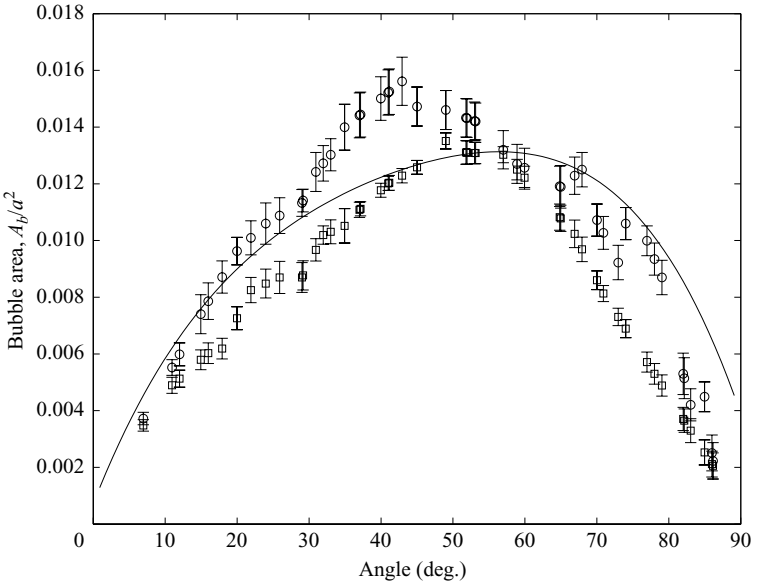

FIGURE 4. Comparison of the vapour cavity size in-between the cylinder wall and the smooth (circles) and the roughest (squares) 25 mm diameter steel spheres. Angle represents the sphere position up the wall, defined in figure 1. Bubble area is the measured viewable area (projected as a disk) of the cavitation bubble, normalized by the square of the sphere radius. The fluid is glycerine at 23.6 °C. The solid curve represents the theoretical predictions of Ashmore *et al.* (2005).

which the predicted gap width exceeds the maximum rough asperity sizes are 21°, 31° and 55° respectively, but it is unclear whether the predicted gap should be compared to the distance from the cylinder surface to the maximum asperity height, the average asperity height or the sphere's core diameter. Coefficients of friction can be found for the three roughened spheres by taking the tangent of the angle at which slip first occurs. They are 0.194 ± 0.036, 0.231 ± 0.037 and 0.270 ± 0.037 respectively for the $\epsilon = 84 \times 10^{-6}$, 164×10^{-6} and 440×10^{-6} spheres. The roughened spheres continued to achieve a steady state according to the hydrodynamical theory until the cylinder rotation rate was increased sufficiently for the spheres' location angle to exceed 90°, whereupon they left the fixed point motion and began to oscillate. Hence, the roughened spheres rotated in accord with the hydrodynamic behaviour of the smooth sphere for a large range of position angles and cylinder surface speeds. Most importantly, the behaviour of the spheres in all three regimes (contact, transition and hydrodynamic) was found to be both continuous and reversible, i.e. no hysteretic behaviour was found with increasing and decreasing cylinder surface speed. The size of the bubble is defined as its measured area when viewed through the cylinder wall. Estimates for the size of the vapour cavity for the roughest sphere are plotted as a function of angular location of the fixed points in figure 4. It is interesting to note that the bubble size is little affected by the roughness. The cavitation bubble was always found in the same position and approximately the same size as for the case of the smooth sphere. This suggests that there was a continuous flow of fluid around the rough asperities capable of creating the pressure distribution required to cause cavitation even in the contact regime.

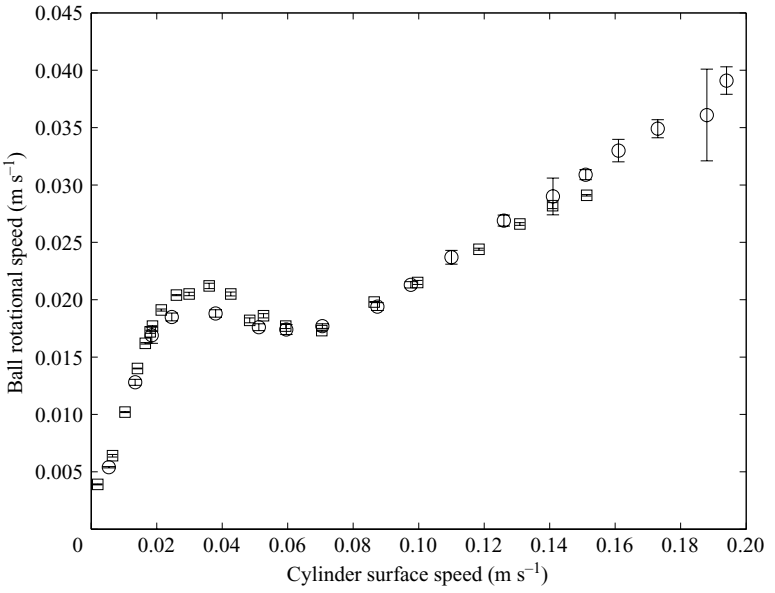

FIGURE 5. Relationship between the cylinder surface speed and sphere rotational speeds for 15.8 mm rough sphere in glycerine (squares) and silicone oil (circles).

The depth of the lubrication layer between the smooth sphere and cylinder wall is estimated to be ∼0–50 μm using the model of Ashmore *et al.* (2005), with a pressure variation of ±1 MPa. For roughened spheres in the crossover regime the lubrication depth will be between that predicted for the hydrodynamic limit and particle–boundary contact. The corresponding pressure variation will significantly increase from ±1 MPa as contact is approached and pressure-dependent effects of viscosity may become important. For such effects to be significant the pressure variation must exceed 100 MPa (Kapitza 1965; Cook *et al.* 1994). To test whether the sphere motion was affected by this the experiment was repeated in both glycerine ($T = 20.4 \pm 0.1\,^{\circ}\mathrm{C}$) and silicone oil ($T = 21.8 \pm 0.1\,^{\circ}\mathrm{C}$). At these temperatures the two fluids have similar viscosities at atmospheric pressure ($\nu = 1095 \pm 10\,\mathrm{mm^2\,s^{-1}}$ for glycerine and $\nu = 1086 \pm 3\,\mathrm{mm^2\,s^{-1}}$ for silicone oil) but at higher pressures a 50 % increase in the viscosity of silicon oil is achieved at a pressure of 100 MPa compared with 600 MPa for glycerine. Plots of the rotation speed of the 15.8 mm diameter sphere against that of the cylinder for both fluids is shown in figure 5. Both sets of data overlay each other showing that any effects from the pressure dependence of viscosity are negligible.

An investigation of the effects of dissolved air in the system was carried out by repeating the experiment with the smooth 25 mm sphere without degassing the fluid. The reduced pressure required to form a bubble from dissolved gases in the fluid is considerably less than for a vapour cavity and hence the observed bubble is expected to be larger. Images are shown in figure 6 of the cavitation bubble for both a degassed and a gassy system. The gas bubble was saturated with air and had an area approximately 8 times larger than the cavitation bubble in the degassed system. The streamwise diameter and, hence, the visible area of an air bubble can be predicted by finding the radii at which the pressure distribution given by the model of Ashmore *et al.* (2005) and the saturation pressure for air in glycerine (∼5 kPa) cross. Using this method, the theoretical relative size of the air bubble to the vapour bubble is found to be 8.03, in good agreement with the measured value. When reducing the cylinder

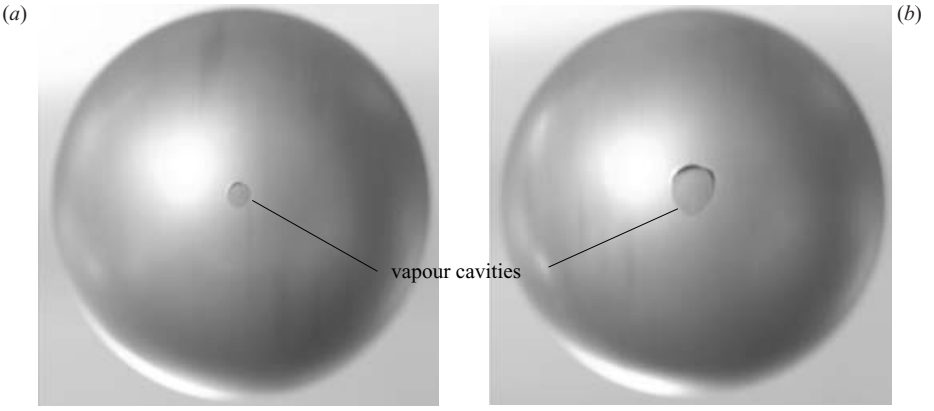

FIGURE 6. Images of the cavitation bubble for a degassed experiment (*a*) and an experiment where the fluid had not been degassed (*b*). The sphere is a 25 mm roughened steel sphere and the rotation directions of sphere and cylinder surface are bottom to top. The fluid is glycerine at 23.6 °C. These images were recorded through the cylinder wall adjacent to the sphere, perpendicular to the point of closest approach.

rotation rate to zero and allowing the sphere to come to rest, the cavitation bubble collapsed and the dissolved air was released and floated to the top of the cylinder, as reported by Prokunin (2004). No difference was detected in the relationship between cylinder surface speed and sphere rotational speed in either system. Hence the bubble has little effect on the tangential force and its primary role is in facilitating a net normal force. The weak effect of the different bubble size on the tangential force and torque is consistent with their known logarithmic dependence on the sphere–boundary separation (Goldman *et al.* 1967).

5. Conclusions

We have observed the effects of surface roughness on spheres moving near to a boundary in a Stokes flow in a rotating cylinder. Smooth spheres move in the hydrodynamical regime described by Ashmore *et al.* (2005).

At low cylinder rotation rates the roughened spheres rotate at the same rate as the cylinder, indicating particle–boundary contact. As the cylinder rotation rate is increased the spheres slip with respect to the cylinder wall and there is a continuous crossover from the particle–boundary contact regime and the hydrodynamic limit.

The hydrodynamic regime, in which roughness effects are negligible, is understood. The symmetry of the problem is broken by the truncation of the pressure distribution at the vapour pressure in the lubricating layer. Here we have shown that the vapour cavity in the system is robust to roughness level and system impurities, such as dissolved air. The size of the cavitation bubble does not appear to have a significant effect on the motion of the sphere.

The model of Smart *et al.* (1993) cannot be used to explain the results presented here for heavy spheres. Their model predicts that the particle–boundary contact regime reaches the hydrodynamical limit (transition 2 in our nomenclature) at a sphere position angle of 90°, whereas this is found to occur at much less than 90° experimentally (∼26° for the roughest 25 mm sphere). The effect that surface roughness has on the flow dynamics is a complicated issue and the possibility of including cavitation in the model of Smart *et al.* (1993) is left open.

L. Y. is supported by a grant from the Chinese Government, J. S. by a grant from the EPSRC, T. M. by an EPSRC Senior Fellowship, C. dP. by a grant from the Andalusian Government and J. A. by a grant from the Leverhulme Trust.

REFERENCES

Acheson, D. J. 1990 *Elementary Fluid Dynamics*. Oxford University Press.

Ashmore, J., del Pino, C. & Mullin, T. 2005 Cavitation in a lubricating flow between a moving sphere and a boundary. *Phys. Rev. Lett*. **94**, 124501.

Cook, R. L., King Jr., H. E., Herbst, C. A. & Herschback, D. R. 1994 Pressure and temperature dependent viscosity of two glass forming liquids: Glycerol and dibutyl phthalate. *J. Chem. Phys.* **100**, 5178–5189.

Dowson, D. & Taylor, C. 1979 Cavitation in bearings. *Annu. Rev. Fluid Mech.* **11**, 35–65.

Galvin, K. P., Zhao, Y. & Davis, R. H. 2001 Time-averaged hydrodynamic roughness of a noncolloidal sphere in low Reynolds number motion down an inclined plane. *Phys. Fluids* **13**, 3108–3119.

Goldman, A. J., Cox, R. G. & Brenner, H. 1967 Slow viscous motion of a sphere parallel to a plane wall-I Motion through a quiescent fluid. *Chem. Engng Sci.* **22**, 637–651.

Kaptiza, P. 1965 *Collected Papers of P. L. Kapitza, Vol. II (1938–1964)* (ed. D. ter Haar). Macmillan.

Mullin, T., Li, Y., del Pino, C. & Ashmore, J. 2005 An experimental study of fixed points and chaos in the motion of spheres in a Stokes flow. *J. Appl. Maths* **70**, 666–676.

Prokunin, A. N. 2004 Microcavitation in the slow motion of a solid spherical particle along a wall in a fluid. *Fluid Dyn.* **39**, 771–778.

Segre, P. N., Herbolzheimer, E. & Chaikin, P. M. 1997 Long-range correlations in sedimentation. *Phys. Rev. Lett*. **79**, 2574–2577.

Smart, J. R., Beimfohr, S. & Leighton, D. T. 1993 Measurement of the translational and rotational velocities of a noncolloidal sphere rolling down a smooth inclined plane at low Reynolds number. *Phys. Fluids* A **5**, 13–24.